High-pressure synthesis and magnetic properties of $Gd_2Rh_3Al_9$ with a distorted honeycomb lattice

Hiroaki HAYASHI,[1,2,*] Xun KANG,[1,2] Alexei BELIK,[1] Hiroyuki K. YOSHIDA,[3]
and
Kazunari YAMAURA [1,2]

[1] Research Center for Materials Nanoarchitectonics (MANA), National Institute for Materials Science, 1-1 Namiki, Tsukuba, Ibaraki 305-0044, Japan
[2] Graduate School of Chemical Sciences and Engineering, Hokkaido University, Sapporo, Hokkaido 060-8628, Japan
[3] Department of Physics, Faculty of Science, Hokkaido University, Sapporo, Hokkaido 060-0810, Japan

* Corresponding author.
Hiroaki HAYASHI
Quantum Solid State Materials Group
Research Center for Materials Nanoarchitectonics (MANA)
National Institute for Materials Science
1-1 Namiki, Tsukuba, Ibaraki 305-0044, Japan
E-mail: Hayashi.hiroaki@nims.go.jp

Abstract:

This study focuses on exploring new Gd-based intermetallic compounds with honeycomb structures to elucidate intriguing magnetic phenomena, particularly the presence of magnetic skyrmions. The compound $Gd_2Rh_3Al_9$, synthesized via high-temperature and high-pressure methods, exhibits an orthorhombic structure characterized by a distorted Gd-honeycomb network. Comprehensive investigations of its temperature-dependent behavior in polycrystalline samples reveal sequential antiferromagnetic transitions occurring at T_1 = 13.6 K and T_2 = 4.1 K. These transitions arise from the antiferromagnetic interaction between the magnetic moments of Gd^{3+} (S = 7/2) situated within the distorted honeycomb layer. Despite not observing a skyrmion phase in this compound, the data provide valuable insights into the complex behavior of Gd-based intermetallic compounds and their potential as hosts for novel magnetic phases. Further research, particularly using single crystals, is needed to explore the possibility of forming a skyrmion phase in this compound.

Keywords:

$Gd_2Rh_3Al_9$, Intermetallic compounds, High-pressure synthesis, Magnetic skyrmion

1. Introduction

The magnetic properties of 4f electron systems are often attributed to the Ruderman-Kittel-Kasuya-Yosida (RKKY) interaction, arising from the coupling between localized 4*f*-electron spins and the spin polarization of conduction electrons. In Gd-based intermetallic compounds, Gd^{3+} ions possess no orbital moments, leading to the absence of a crystalline electric field, and thus, an expectation of isotropic RKKY interactions. However, these compounds can still exhibit magnetic anisotropy, attributed to either permissible single ion anisotropy or contributions from magnetic dipole interactions [1]. This anisotropy results in a diverse range of magnetic structures, such as helical, spiral, and conical arrangements [2–4]. A particularly intriguing phenomenon is the formation of topologically stable magnetic skyrmions, which are distinguished by their unique spin textures.

Recent theoretical studies have significantly expanded our understanding of magnetic skyrmions. These studies have shown that skyrmions can exist not only in systems lacking inversion symmetry, as predominantly observed previously, but also in systems with inversion symmetry [5–9]. Additionally, a novel stabilization mechanism for magnetic skyrmions in inversion symmetric structures has been proposed [10–12]. This mechanism is distinct from conventional ones as it does not rely on the interplay between ferromagnetic exchange interactions and the Dzyaloshinski-Moriya interaction, which are typically considered in skyrmion formation [13–15].

Significantly, the majority of magnetic skyrmions recently discovered in material systems with inversion symmetry are found in layered compounds [5,6,13–18]. This is because multiple propagation vectors are energetically equivalent and become degenerate due to rotational operations. For instance, the single-*Q* magnetic state in Gd_2PdSi_3 [5,6,13,15,18] and $Gd_3Ru_4Al_{12}$ [6,14,16–18] exhibits triple degeneracy on a triangular lattice, which facilitates the formation of triangular skyrmion lattices. Similarly, in $GdRu_2Si_2$ [7,8,19–21], square skyrmion lattices emerge due to quadruple degeneracy on the square lattice. Consequently, multi-*Q* states demonstrate enhanced stability in lattices with high rotational symmetry.

While the high rotational symmetry of layered structures suggests the stabilization of skyrmion lattices, skyrmion lattices have also been observed in distorted lattices. For example, tetragonal $EuAl_4$ exhibits a structural transition to an orthorhombic lattice at low temperatures. This transition results in Eu^{2+} layers breaking their four-fold rotational symmetry, yet a rhombic skyrmion lattice still emerges [9]. Additionally, theoretical studies have been conducted on the effects of orthorhombic distortion on skyrmion stabilization [22]. Experimental verification is needed to support these theoretical findings.

In this study, our emphasis lies in the quest for intermetallic compounds featuring distorted crystal structures, aiming to uncover potential magnetic skyrmions. A notably auspicious candidate in this context is a Gd-based intermetallic compound of $Y_2Co_3Ga_9$-type, wherein Gd takes

the place of Y, existing within a subtly distorted honeycomb lattice. This suggests its viability as a host material for magnetic skyrmions [23–25]. As a stride towards this objective, we synthesized $Gd_2Rh_3Al_9$ by substituting Rh for Co and Al for Ga. This paper provides an account of the synthesis of this $Gd_2Rh_3Al_9$ compound of $Y_2Co_3Ga_9$-type, detailing its crystal structure, essential magnetic properties, and electrical conduction behavior. The findings provide insights into the characteristics of this compound and its potential as a platform for investigating distinct magnetic states.

2. Experimental

Polycrystals and single crystals of $Gd_2Rh_3Al_9$ were synthesized using the Al self-flux method under high-pressure and high-temperature conditions. The raw materials, Gd, Rh, and Al, were combined in a molar ratio of 2:3:9.9 and encapsulated within a BN capsule. This assembly was then enclosed in an outer capsule made of Ta. The entire capsule arrangement was placed within a multi-anvil high-pressure apparatus (CTF-MA1500P; C&T Factory Co., Ltd., Tokyo, Japan) and subjected to heating at 1600 °C for 1 hour. Subsequently, a gradual cooling process occurred over 2 hours, reaching 900 °C, while maintaining a pressure of 6 GPa.

Following the heating steps, rapid cooling procedures brought down the capsule's temperature to below 100 °C in less than 30 seconds. Subsequently, the pressure was methodically released over a 2-hour period. The resulting product comprised gleaming grey crystals clustered at the lowermost section of the BN capsule, alongside a polycrystalline segment that formed in the major region of the sample. The crystals from the former category underwent physical fragmentation, yielding minute crystals akin to single domains, with dimensions not exceeding 0.2 mm (Fig. 1a). Maintaining high-pressure conditions was essential in this synthesis. Without such conditions, achieving the desired chemical phase would not have been possible.

Crystallographic data were obtained from a carefully selected crystal, which had been polished and cleaned to eliminate any potential residue of Al flux. These data were analyzed using a Rigaku XtaLab mini II diffractometer, which employed Mo Kα radiation. The crystal structure was initially elucidated using the dual-space algorithm approach of SHELXT [26], followed by further refinement through a full-matrix least-squares method using SHELXL. This refinement process was facilitated by the Olex graphical user interface. The detailed results derived from this comprehensive analysis are thoroughly documented in Tables I and II.

Additionally, we conducted Scanning Electron Microscope-Energy Dispersive X-ray Spectroscopy (SEM-EDX) measurements on a polished surface of the selected specimen, mounted on carbon tape. This analysis, performed using a TESCAN Vega-e SBU scanning electron microscope equipped with EDS and operating at an accelerating voltage of 15 kV, yielded the elemental ratio Gd: Rh: Al = 1.73(4): 3.10(4): 9.17(5). These results indicate that the ratio of Gd is

slightly lower than the stoichiometry of Gd2Rh3Al9, as further detailed in the Supporting Information. However, we believe this discrepancy is more likely attributable to instrumental precision issues rather than a significant deviation from the intended stoichiometry.

Magnetic susceptibility (χ) and isothermal magnetization (M) measurements were carried out across a temperature range spanning from 2 K to 300 K, employing magnetic fields up to 70 kOe. These analyses were performed using a SQUID magnetometer MPMS3 (Quantum Design, Inc.). To assess specific heat capacity (C_p) and direct current electrical resistivity (ρ), we employed a relaxation method and a four-probe technique, respectively. These experimental procedures were conducted utilizing a PPMS (Quantum Design Inc.).

It is crucial to note that the limited size of the single-domain-like crystals made it infeasible to perform assessments of physical properties along specific crystal directions using our measurement apparatus. Therefore, except for the structural study, all other measurements were conducted on polycrystalline samples. Powder X-ray diffraction (XRD) analysis, the pattern of which is provided in the Supporting Information, identified a small amount of RhO_2 as an impurity in the polycrystalline sample. However, given that RhO_2 is nonmagnetic and exhibits metallic electrical conductivity within our measurement temperature range, we concluded that the intrinsic properties of $Gd_2Rh_3Al_9$ are not significantly affected by the presence of RhO_2.

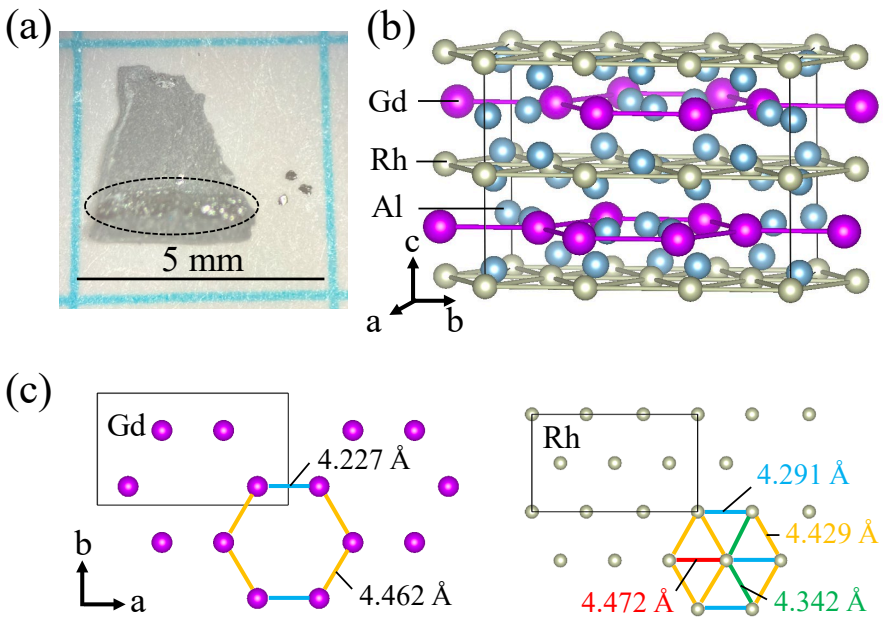

Fig. 1: (a) Photograph depicting a $Gd_2Rh_3Al_9$ sample synthesized under high pressure. The dotted ellipse delineates a clustered area of single crystals formed at the bottom of the BN capsule. Adjacent to the sample are crystal fragments detached from this area. The region above the dotted

area is polycrystalline. (b) Schematic representation of the crystal structure of $Gd_2Rh_3Al_9$, displaying its orthorhombic structure (*Cmcm*). (c) View of the Gd-honeycomb lattice and Rh-triangular lattice from the c-axis direction. The numbers indicate interatomic distances, revealing slight distortions from the ideal lattice.

Table I: Crystallographic parameters and refinement details of a single crystal of $Gd_2Rh_3Al_9$

Empirical formula	$Gd_2Rh_3Al_9$
Formula weight	866.05
Temperature	293(2) K
Wavelength	0.71073 Å (Mo K_α)
Crystal system	Orthorhombic
Space group	*Cmcm*
Unit cell dimensions	a = 13.0538(4) Å, b = 7.6455(3), c = 9.5117(3) Å
Volume	949.29(6) $Å^3$
Z	4
Density (calculated)	6.060 g cm^{-3}
Absorption coefficient	19.649 mm^{-1}
F_{000}	1520
Crystal size	0.066 × 0.056 × 0.024 mm^3
2θ for data collection	3.0710 – 30.4550°
Index ranges	$-16 \le h \le 18$, $-10 \le k \le 10$, $-13 \le l \le 13$
Reflections collected	7294
Independent reflections	793 [R(int) = 0.0313]
Completeness to θ = 25.242°	100%
Absorption correction	multi-scan
Max. and min. transmission	1.000 and 0.738
Data/restraints/parameters	793/0/42
Goodness-of-fit on F^2	1.064
Final R indices [$I > 2\sigma(I)$]	R_1 = 0.0147, wR_2 = 0.0285
R indices (all data)	R_1 = 0.0178, wR_2 = 0.0291
Extinction coefficient	0.00068(3)
Largest diff. peak and hole	1.088 and –0.721 e $Å^{-3}$

Table II: Atomic coordinates and equivalent isotropic displacement parameters (U_{eq}, 10^{-3} Å^2) and anisotropic displacement parameters (U_{ij}; 10^{-3} Å^2) as measured by X-ray diffraction on a single-crystal $Gd_2Rh_3Al_9$ at 293 K.

Site	WP [a]	Occp.	*x*	*y*	*z*	U_{eq} [b]
Gd	8*g*	1	0.65998(2)	0.83145(2)	1/4	5.69(6)
Rh1	8*e*	1	0.67087(2)	1/2	1/2	4.55(7)
Rh2	4*b*	1	1/2	0	1/2	4.58(8)
Al1	8*f*	1	1/2	-0.1279(2)	0.0067(3)	6.7(3)
Al2	8*g*	1	0.60687(9)	0.44226(14)	1/4	7.2(2)
Al3	16*h*	1	0.83185(6)	0.66700(11)	0.42572(9)	6.24(16)
Al4	8*f*	1	1/2	0.33228(14)	0.54338(12)	8.6(2)
Site	U_{11}	U_{22}	U_{33}	U_{23}	U_{13}	U_{12}
Gd	6.00(10)	5.95(9)	5.12(8)	0	0	0.51(7)
Rh1	3.76(15)	5.11(14)	4.77(13)	-0.37(11)	0	0
Rh2	4.44(19)	4.56(18)	4.73(16)	0.89(15)	0	0
Al1	4.5(8)	9.1(8)	6.5(7)	0	0	0
Al2	7.5(6)	8.2(5)	5.9(5)	0	0	-1.1(4)
Al3	5.2(4)	6.9(4)	6.6(3)	-0.5(3)	0.5(3)	-0.3(3)
Al4	4.2(6)	6.1(5)	15.6(5)	0.1(5)	0	0

[a] Wyckoff positions

[b] U_{eq} is defined as one third of the trace of the orthogonalized U_{ij} tensor. The anisotropic displacement factor exponent takes the form $-2\pi^2[h^2a^{*2}U_{11} + ... + 2hka^*b^*U_{12}]$.

3. Results and Discussions

The crystal structure of $Gd_2Rh_3Al_9$ was confirmed by XRD analysis to possess a $Y_2Co_3Ga_9$-type structure (*Cmcm*, #63), akin to $Gd_2Co_3Al_9$ [25]. The Gd-honeycomb layers are aligned along the c-axis (Fig. 1b). Within the intralayer structure, the hexagons constituting the honeycomb network display subtle contractions along the a-axis. These hexagons are comprised of edges with two distinct bond lengths, measuring 4.227 Å and 4.429 Å, respectively (Fig. 1c, left side). Similarly, the triangles formed by Rh in the subsequent layers exhibit distortions, encompassing four isosceles triangles and eight non-equilateral triangles within the unit cell (Fig. 1c, right side). These minor deviations may stem from the overall structure of the orthorhombic crystal, which exhibits a slight departure from trigonal or hexagonal symmetry.

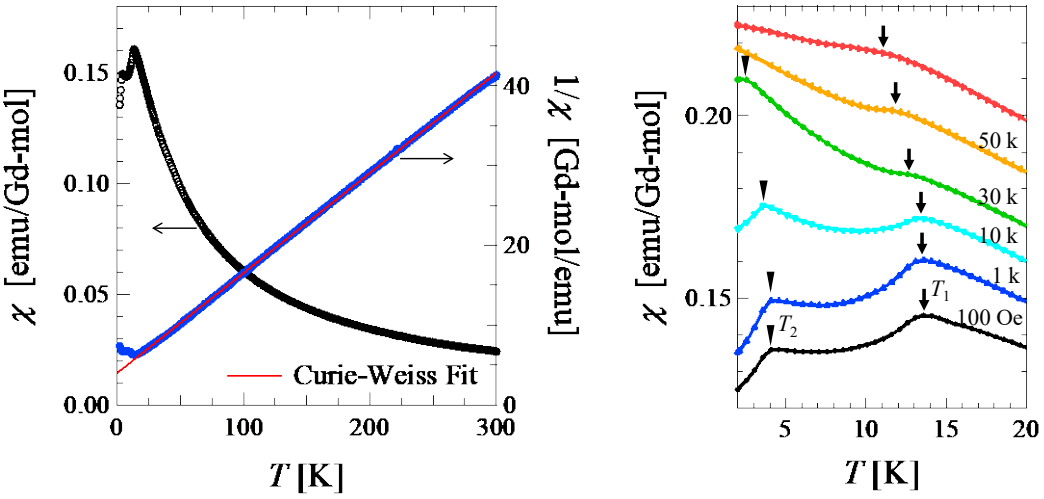

Fig. 2: (a) Temperature dependence of χ and $1/\chi$ under H = 1 kOe. The solid red line represents the Curie-Weiss fit for the data above 50 K. (b) χ below 20 K under several magnetic fields ranging from 100 Oe to 70 kOe. Arrows and triangular symbols indicate the anomalies at T_1 and T_2, respectively.

The temperature-dependent behavior of χ under H = 1 kOe is depicted in Fig. 2a. The inverse of χ conforms well to the Curie-Weiss law, represented by $1/\chi = (T - \theta_W)/C$, for temperatures exceeding 50 K. The Curie constant, C, is calculated to be 7.973(5) emu K mol^{-1}. The corresponding effective moment, p_{eff} = 7.984(2) μ_B, closely aligns with the anticipated value of 7.94 μ_B for free Gd^{3+} ions with S = 7/2. The Weiss temperature, θ_W, is determined to be -32.0(1) K, indicating that the predominant interaction between the magnetic moments of Gd^{3+} ions is of an antiferromagnetic nature.

Upon lowering the temperature, a magnetic transition manifested at T_1 in the χ vs T measurements, followed by another distinctive anomaly indicating an additional magnetic transition at a lower temperature, labeled as T_2. Notably, consecutive peaks were discerned at T_1 = 13.6 K and T_2 = 4.1 K at H = 100 Oe. These transition temperatures exhibited minor shifts towards the lower temperature range with the progressive increase of the magnetic field, extending up to H = 70 kOe, as illustrated in Fig. 2b. Considering T_1 as a representative of a long-range antiferromagnetic transition temperature, the corresponding frustration parameter $|\theta_W|/T_1$ was calculated to be 2.34. This value aligns with the range (typically 1-3) often reported for Gd-based intermetallic compounds known to accommodate skyrmions [27–29]. However, the negative θ_W observed here is in considerable contrast to the positive θ_W (20-64 K) reported for other Gd-based intermetallic compounds [27–29].

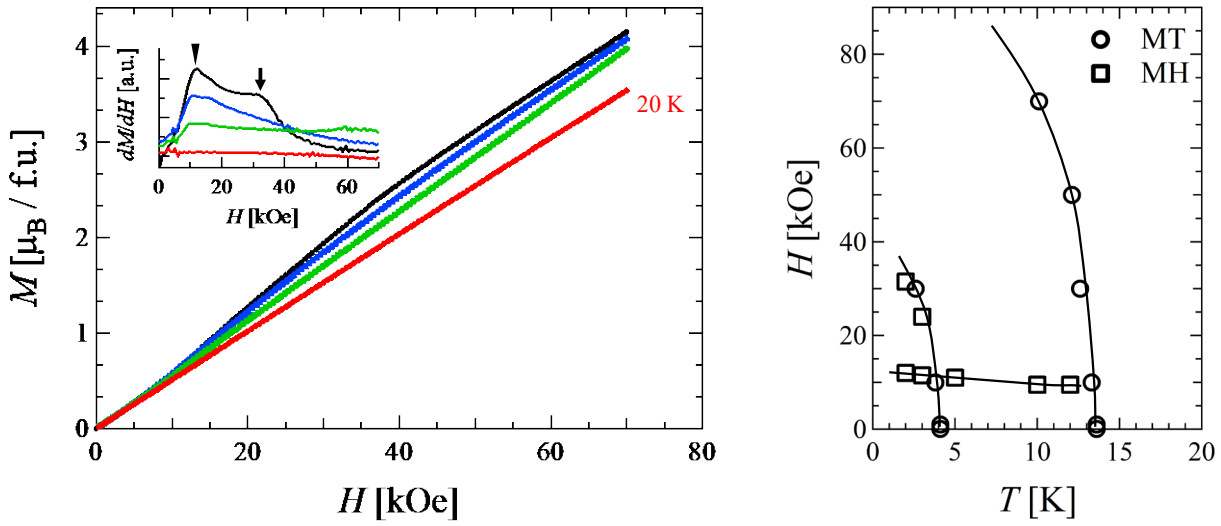

Fig. 3: (a) Isothermal M curves below 20 K. The inset shows the differential of M (dM/dH) at each temperature. Arrows within the inset highlight transition points. (b) The magnetic field-temperature phase diagram for $Gd_2Rh_3Al_9$, which is constructed based on the data from our magnetic measurements.

Figure 3 (a) illustrates the isothermal M curves acquired within the temperature range of 2 K to 20 K. Notably, two distinct anomalies are prominently observed at approximately H_1 = 15 kOe and H_2 = 30 kOe. These anomalies are clearly depicted in the differential curves of M at 2 K, as showcased in the inset of Fig. 3. The anomaly at H_1 materializes below T_1, while the anomaly at H_2 emerges beneath T_2. This observation indicates that the former anomaly is linked to the antiferromagnetic structure formed at T_1, while the latter pertains to the magnetic arrangement existing below T_2. The M value of 4.2 μ_B recorded at 70 kOe under 2 K equates to approximately 60% of the saturation moment exhibited by spins with S = 7/2. However, it is noteworthy that no distinctive step-like anomalies accompanied by magnetic hysteresis, commonly observed in skyrmion compounds [18,27–29], were discerned in this case. The complex phase diagram, dependent on magnetic field and temperature, derived from our magnetization-temperature (M-T) and magnetization-field (M-H) measurements, is presented in Fig. 3 (b).

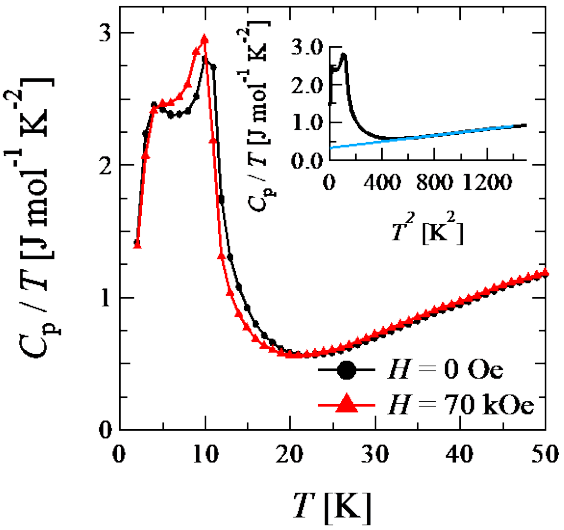

Fig. 4: Temperature dependence of C_p/T under $H = 0$ and 70 kOe. Transition temperatures, T_1 and T_2, are indicated by an arrow and a triangular symbol, respectively. The inset displays the C_p/T vs. T^2 plot, with the blue line denoting the outcome of linear fitting.

The temperature-dependent behavior of C_p is investigated under magnetic fields of 0 and 70 kOe, as depicted in Fig. 4. The C_p/T data at zero-field reveals magnetic transitions corresponding to T_1 and T_2. Notably, the peak associated with T_1 shifts towards lower temperatures with the increment of magnetic fields, extending up to 70 kOe. The inset of Fig. 4 illustrates a plot of C_p/T versus T^2, wherein a linear fitting is applied based on the equation $C_p/T = \gamma + \beta T^2$. Here, γ represents the electronic specific heat coefficient, and β is a constant associated with the Debye temperature Θ_D. The data above T_1 are subjected to fitting, effectively circumventing the influence of the magnetic phase transition. The Sommerfeld coefficient γ is ascertained to be 328 mJ mol^{-1} K^{-2}. While this value surpasses those observed in other Gd-based intermetallic compounds, it remains comparable to the reported value of 500 mJ mol^{-1} K^{-2} in $Gd_2Co_3Al_9$ [25]. The Debye temperature Θ_D is calculated to be 168 K based on the estimated β.

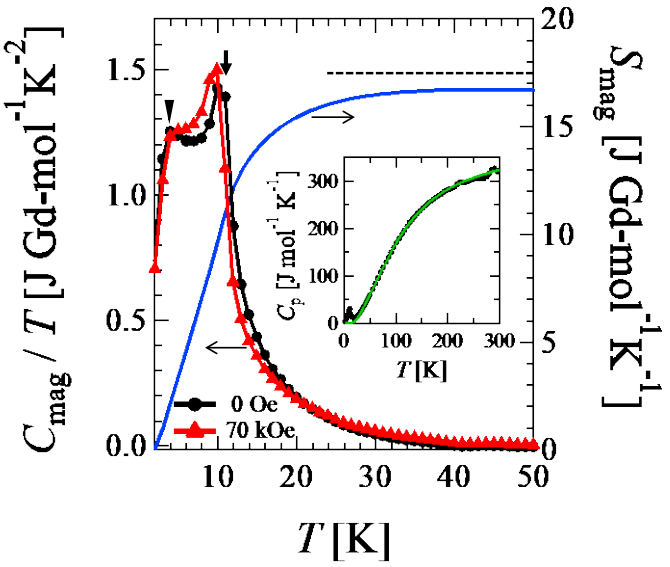

Fig. 5: Temperature dependence of C_{mag}/T under H = 0 Oe (black) and 70 kOe (red), and magnetic entropy (blue line). Transition temperatures, T_1 and T_2, are indicated by an arrow and a triangular symbol, respectively. The inset displays the C-T plot, with the green line denoting the fitting by the Einstein-Debye formula.

The inset of Fig. 5 shows the zero-field (H = 0 Oe) C_p curve and lattice contribution calculated from the Einstein-Debye function, which exhibits great fitting for temperatures exceeding 40 K except in the noisy region (250-300 K) due to the sample-fixing grease. The fitting function is described as follows:

$$C_p = \gamma T + 3n_E R\frac{x^2e^x}{(e^x-1)^2} + 9n_D R(\frac{T}{\theta_D})^3 \int_0^{\theta_D/T} \frac{y^4e^y}{(e^y-1)^2}dy$$

Here, the first term represents a conduction electron contribution, where γ is the Sommerfeld coefficient. The second and third terms correspond to a phonon contribution following Einstein's and Debye's models, respectively. In the equations, $x = \theta_E/T$, $y = \theta_D/T$, in which θ_E and θ_D are the Einstein and Debye temperatures, respectively. The numbers of Einstein models (n_E) and Debye oscillations (n_D) are constrained by $n_E + n_D = 14$ (the number of atoms per formula unit).

In this case, proper fitting is observed with the following parameters: γ = 16.7(17) mJ mol^{-1} K^{-2}, n_E = 3.1(1), θ_E = 148(3) K, n_D = 10.9(1), and θ_D = 493(3) K. The estimated γ and θ_D are much smaller and larger, respectively, than those reported for the isostructural compound $Gd_2Co_3Al_9$ (γ = 500 mJ mol^{-1} K^{-2}, θ_D = 187 K) [25]. Previous studies on $Gd_2Co_3Al_9$ relied solely on the approximate formula $C_p/T = \gamma + \beta T^2$ to estimate these values, potentially making it challenging to accurately isolate the contribution from the magnetic transition. This discrepancy underscores the critical role

of fitting methods in precisely determining thermodynamic parameters.

To better understand the magnetic properties, the magnetic specific heat divided by T (C_{mag}/T) and magnetic entropy (S_{mag}), by subtracting lattice contribution from C_p, are shown in Fig. 5. The C_{mag}/T data at zero-field reveals magnetic transitions corresponding to T_1 and T_2. Notably, the peak associated with T_1 shifts towards lower temperatures with the increment of magnetic fields extending up to 70 kOe. The S_{mag} in zero field estimated by integrating the C_{mag}/T data with respect to T reaches 96.6 % of the expected value Rln8 for S= 7/2 and saturates to Rln8 at around 50 K.

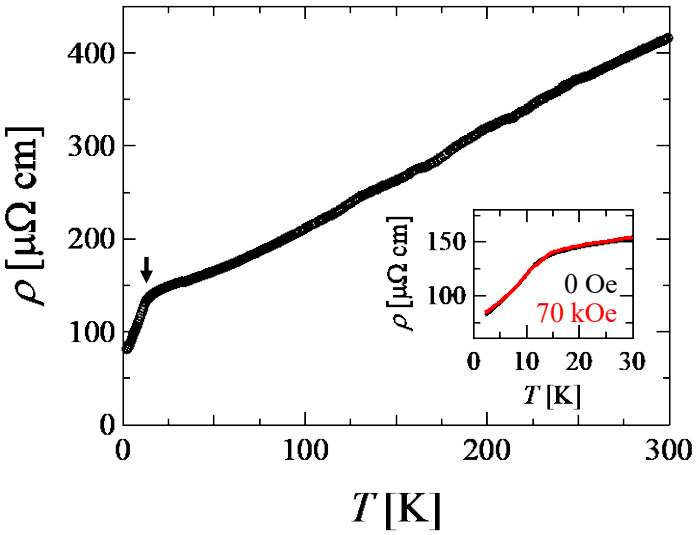

Fig. 6: Temperature dependence of ρ below 300 K under zero magnetic field. The inset shows the ρ curves under H = 0 and 70 kOe.

Figure 6 presents the temperature-dependent behavior of ρ under zero magnetic field and at 70 kOe for $Gd_2Rh_3Al_9$. In both scenarios, the curves show a sudden decline just below T_1, which is likely due to the influence of the antiferromagnetic ordering process. Notably, while a distinctive hump in the ρ curve, indicative of a transition to a skyrmion phase, has been observed in $GdRu_2Si_2$ [30], no analogous anomaly is evident in $Gd_2Rh_3Al_9$. The residual resistivity ratio (RRR) of the compound is calculated to be 5.1. This suggests that there may be contributions from grain boundary scattering in the polycrystalline sample [31], or it could imply that the sample quality is not at its optimal level.

4. Conclusion

We have achieved a significant milestone in synthesizing the Gd-based intermetallic compound $Gd_2Rh_3Al_9$ through high-temperature and high-pressure synthesis. Crystal structure

analysis revealed an orthorhombic structure characterized by a distorted Gd-honeycomb network. A comprehensive study of the temperature-dependent behavior of χ, M, C_p, and ρ, in polycrystalline samples revealed sequential antiferromagnetic transitions occurring at T_1 = 13.6 K and T_2 = 4.1 K. These transitions are ascribed to the antiferromagnetic interactions between the magnetic moments of Gd^{3+} (S = 7/2) within the distorted honeycomb layers. The magnetic phase diagram derived from these findings exhibits a complex dependence on temperature and magnetic field, suggesting the presence of various magnetically ordered states.

However, our study did not provide evidence for the existence of a skyrmion phase in this compound. This may be attributed, at least in part, to the significantly stronger antiferromagnetic interactions compared to other Gd-based skyrmion materials. Nevertheless, the data on the magnetic and transport properties of $Gd_2Rh_3Al_9$ obtained in this study offer valuable insights into the intricate behavior of Gd-based intermetallic compounds and their potential as hosts for unique magnetic phases. Furthermore, conducting detailed measurements using single crystals is imperative to further explore the possibility of forming a skyrmion phase in this compound. This remains a subject for future research.

Acknowledgment

We thank H. Sakurai and Y. Tsujimoto for helpful discussion. MANA is supported by the World Premier International Research Center Initiative (WPI) of MEXT, Japan. This research was partly funded by a Grant-in-Aid for Scientific Research from the Japan Society for the Promotion of Science (No. JP22H04601) and the Kazuchika Okura Memorial Foundation (No. 2022-11).

References

[1] M. Rotter, M. Loewenhaupt, M. Doerr, A. Lindbaum, H. Sassik, K. Ziebeck, B. Beuneu, Dipole interaction and magnetic anisotropy in gadolinium compounds, Phys Rev B. 68 (2003). https://doi.org/10.1103/PhysRevB.68.144418.

[2] M.A. Ruderman, C. Kittel, Indirect Exchange Coupling of Nuclear Magnetic Moments by Conduction Electrons, Physical Review. 96 (1954). https://doi.org/https://doi.org/10.1103/PhysRev.96.99.

[3] T. Kasuya, A Theory of Metallic Ferro-and Antiferromagnetism on Zener's Model, Progress of Theoretical Physics. 16 (1956). https://doi.org/https://doi.org/10.1143/PTP.16.45.

[4] K. Yosida, Magnetic Proyerties of Cu-Mn Alloys, Physical Review. 106 (1957). https://doi.org/https://doi.org/10.1103/PhysRev.106.893.

[5] T. Kurumaji, T. Nakajima, M. Hirschberger, A. Kikkawa, Y. Yamasaki, H. Sagayama, H. Nakao, Y. Taguchi, T. Arima, Y. Tokura, Skyrmion lattice with a giant topological Hall effect in a frustrated triangular-lattice

magnet, Science (1979). 365 (2019) 914–918. https://doi.org/DOI: 10.1126/science.aau0968.

[6] M. Hirschberger, T. Nakajima, S. Gao, L. Peng, A. Kikkawa, T. Kurumaji, M. Kriener, Y. Yamasaki, H. Sagayama, H. Nakao, K. Ohishi, K. Kakurai, Y. Taguchi, X. Yu, T. Arima, Y. Tokura, Skyrmion phase and competing magnetic orders on a breathing kagomé lattice, Nat Commun. 10 (2019) 5831. https://doi.org/10.1038/s41467-019-13675-4.

[7] N.D. Khanh, T. Nakajima, S. Hayami, S. Gao, Y. Yamasaki, H. Sagayama, H. Nakao, R. Takagi, Y. Motome, Y. Tokura, T. hisa Arima, S. Seki, Zoology of Multiple-Q Spin Textures in a Centrosymmetric Tetragonal Magnet with Itinerant Electrons, Advanced Science. 9 (2022). https://doi.org/10.1002/advs.202105452.

[8] Y. Yasui, C.J. Butler, N.D. Khanh, S. Hayami, T. Nomoto, T. Hanaguri, Y. Motome, R. Arita, T. hisa Arima, Y. Tokura, S. Seki, Imaging the coupling between itinerant electrons and localised moments in the centrosymmetric skyrmion magnet GdRu2Si2, Nat Commun. 11 (2020) 5925. https://doi.org/10.1038/s41467-020-19751-4.

[9] R. Takagi, N. Matsuyama, V. Ukleev, L. Yu, J.S. White, S. Francoual, J.R.L. Mardegan, S. Hayami, H. Saito, K. Kaneko, K. Ohishi, Y. Ōnuki, T. hisa Arima, Y. Tokura, T. Nakajima, S. Seki, Square and rhombic lattices of magnetic skyrmions in a centrosymmetric binary compound, Nat Commun. 13 (2022). https://doi.org/10.1038/s41467-022-29131-9.

[10] T. Okubo, S. Chung, H. Kawamura, Multiple-q states and the Skyrmion lattice of the triangular-lattice Heisenberg antiferromagnet under magnetic fields, Phys Rev Lett. 108 (2012). https://doi.org/10.1103/PhysRevLett.108.017206.

[11] M. Hirschberger, S. Hayami, Y. Tokura, Nanometric skyrmion lattice from anisotropic exchange interactions in a centrosymmetric host, New J Phys. 23 (2021) 023039. https://doi.org/10.1088/1367-2630/abdef9.

[12] S. Hayami, Y. Motome, Square skyrmion crystal in centrosymmetric itinerant magnets, Phys Rev B. 103 (2021). https://doi.org/10.1103/PhysRevB.103.024439.

[13] R. Mallik, E. V Sampathkumaran, P.L. Paulose, H. Sugawarat, H. Sato, Magnetic anomalies in Gd2PdSi3, PRAMANA Journal of Physics. 51 (1998) 505–509. https://doi.org/https://doi.org/10.1016/S0921-4526(98)01129-6.

[14] R.E. Gkandyshevskii, O.R. Strusievicz, K. Cenzual, E. Parthe, Structure of Gd3Ru4AI12, a New Member of the EuMg5.2 Structure Family with Minority-Atom Clusters, Acta Crystal. 49 (1993) 474–478. https://doi.org/https://doi.org/10.1107/S0108768192011510.

[15] S.R. Saha, H. Sugawara, T.D. Matsuda, H. Sato, R. Mallik, E. V Sampathkumaran, Magnetic anisotropy, first-order-like metamagnetic transitions, and large negative magnetoresistance in single-crystal Gd2PdSi3, Phys Rev B. 60 (1999) 12162–12165. https://doi.org/https://doi.org/10.1103/PhysRevB.60.12162.

[16] V. Chandragiri, K.K. Iyer, E. V. Sampathkumaran, Magnetic behavior of Gd3Ru4Al12, a layered compound with distorted kagomé net, Journal of Physics Condensed Matter. 28 (2016). https://doi.org/10.1088/0953-8984/28/28/286002.

[17] S. Nakamura, N. Kabeya, M. Kobayashi, K. Araki, K. Katoh, A. Ochiai, Spin trimer formation in the metallic compound Gd3Ru4Al12 with a distorted kagome lattice structure, Phys Rev B. 98 (2018). https://doi.org/10.1103/PhysRevB.98.054410.

[18] S. Nakamura, N. Kabeya, M. Kobayashi, K. Araki, K. Katoh, A. Ochiai, Magnetic phases of the frustrated

ferromagnetic spin-trimer system Gd3Ru4Al12 with a distorted kagome lattice structure, Phys Rev B. 107 (2023). https://doi.org/10.1103/PhysRevB.107.014422.

[19] M. Slaski, A. Szytula, J. Leciejewicz, A. Zygmunt, MAGNETIC PROPERTIES OF RERu2Si2 (RE = Pr, Nd, Gd, Tb, Dy, Er) INTERMETALLICS, J Magn Magn Mater. 46 (1984) 114–122. https://doi.org/https://doi.org/10.1016/0304-8853(84)90348-2.

[20] A. Garnier, D. Gignoux, N. Iwata, D. Schmitt, T. Shigeoka, F.Y. Zhang, Anisotropic metamagnetism in GdRu2Si2, J Magn Magn Mater. 140–144 (1995) 899–900. https://doi.org/https://doi.org/10.1016/0304-8853(94)00783-7.

[21] N.D. Khanh, T. Nakajima, X. Yu, S. Gao, K. Shibata, M. Hirschberger, Y. Yamasaki, H. Sagayama, H. Nakao, L. Peng, K. Nakajima, R. Takagi, T. hisa Arima, Y. Tokura, S. Seki, Nanometric square skyrmion lattice in a centrosymmetric tetragonal magnet, Nat Nanotechnol. 15 (2020) 444–449. https://doi.org/10.1038/s41565-020-0684-7.

[22] S. Hayami, Orthorhombic distortion and rectangular skyrmion crystal in a centrosymmetric tetragonal host, JPhys Materials. 6 (2023). https://doi.org/10.1088/2515-7639/acab89.

[23] J. Niermann, B. Fehrmann, M.W. Wolff, W. Jeitschko, Preparation and crystal structure of ternary rare-earth platinum metal aluminides R2T3Al9 (T=Rh, Ir, Pd) with Y2Co3Ga9-type structure and magnetic properties of the iridium compounds, J Solid State Chem. 177 (2004) 2600–2609. https://doi.org/10.1016/j.jssc.2004.03.007.

[24] Ch. Routsi, J.K. Yakinthos, Crystal structure and magnetic properties of R2Co3Al9 compounds (R=Y, Pr, Gd, Tb, Dy, Ho, Er, Tm), Journal of Alloys and Compunds. 323–324 (2001) 427–430. https://doi.org/https://doi.org/10.1016/S0925-8388(01)01103-3.

[25] T.P. Rashid, K. Arun, I. Curlik, S. Ilkovic, M. Reiffers, A. Dzubinska, R. Nagalakshmi, Influence of spin fluctuations on the magnetocaloric behavior of Gd2Co3Al9 compound, J Magn Magn Mater. 466 (2018) 283–288. https://doi.org/10.1016/j.jmmm.2018.07.027.

[26] G.M. Sheldrick, SHELXT - Integrated space-group and crystal-structure determination, Acta Crystallogr A. 71 (2015) 3–8. https://doi.org/10.1107/S2053273314026370.

[27] A.W.D. Leishman, R.M. Menezes, G. Longbons, E.D. Bauer, M. Janoschek, D. Honecker, L. Debeer-Schmitt, J.S. White, A. Sokolova, M. V. Milošević, M.R. Eskildsen, Topological energy barrier for skyrmion lattice formation in MnSi, Phys Rev B. 102 (2020). https://doi.org/10.1103/PhysRevB.102.104416.

[28] M. He, G. Li, Z. Zhu, Y. Zhang, L. Peng, R. Li, J. Li, H. Wei, T. Zhao, X.G. Zhang, S. Wang, S.Z. Lin, L. Gu, G. Yu, J.W. Cai, B.G. Shen, Evolution of topological skyrmions across the spin reorientation transition in Pt/Co/Ta multilayers, Phys Rev B. 97 (2018). https://doi.org/10.1103/PhysRevB.97.174419.

[29] H.Y. Yuan, O. Gomonay, M. Kläui, Skyrmions and multisublattice helical states in a frustrated chiral magnet, Phys Rev B. 96 (2017). https://doi.org/10.1103/PhysRevB.96.134415.

[30] T. Samanta, I. Das, S. Banerjee, Comparative studies of magnetocaloric effect and magnetotransport behavior in GdRu2Si2 compound, J Appl Phys. 104 (2008). https://doi.org/10.1063/1.3043558.

[31] G. Reiss, J. Vancea, H. Hoffmann, Grain-Boundary Resistance in Polycrystalline Metals, Phys Rev Lett. 56 (1986) 2100–2103.